

## Research Article

# Antimicrobial and Controlled Release Studies of a Novel Nystatin Conjugated Iron Oxide Nanocomposite

Samer Hasan Hussein-Al-Ali,<sup>1,2</sup> Mohamed E. El Zowalaty,<sup>3,4</sup> Aminu Umar Kura,<sup>4</sup> Benjamin Geilich,<sup>5</sup> Sharida Fakurazi,<sup>4,6</sup> Thomas J. Webster,<sup>5,7</sup> and Mohd Zobir Hussein<sup>8</sup>

<sup>1</sup> Laboratory of Molecular Biomedicine, Institute of Bioscience, Universiti Putra Malaysia, 43400 Serdang, Selangor, Malaysia

<sup>2</sup> Faculty of Pharmacy, Isra University, P.O. Box 22, Amman 11622, Jordan

<sup>3</sup> Department of Environmental Health, Faculty of Public Health and Tropical Medicine, Jazan University, Jazan, Saudi Arabia

<sup>4</sup> Laboratory of Vaccines and Immunotherapeutics, Institute of Bioscience, Universiti Putra Malaysia, 43400 Serdang, Selangor, Malaysia

<sup>5</sup> Departments of Chemical Engineering and Bioengineering, Northeastern University, Boston, MA 02115, USA

<sup>6</sup> Department of Human Anatomy, Faculty of Medicine and Health Sciences, Universiti Putra Malaysia, 43400 Serdang, Selangor, Malaysia

<sup>7</sup> Center of Excellence for Advanced Materials Research, King Abdulaziz University, Jeddah, Saudi Arabia

<sup>8</sup> Materials Synthesis and Characterization Laboratory, Institute of Advanced Technology (ITMA), Universiti Putra Malaysia, 43400 Serdang, Selangor, Malaysia

Correspondence should be addressed to Mohd Zobir Hussein; mzobir@upm.edu.my

Received 22 January 2014; Accepted 24 March 2014; Published 12 May 2014

Academic Editor: Paolo Colombo

Copyright © 2014 Samer Hasan Hussein-Al-Ali et al. This is an open access article distributed under the Creative Commons Attribution License, which permits unrestricted use, distribution, and reproduction in any medium, provided the original work is properly cited.

Nystatin is a tetraene diene polyene antibiotic showing a broad spectrum of antifungal activity. In the present study, we prepared a nystatin nanocomposite (Nyst-CS-MNP) by loading nystatin (Nyst) on chitosan (CS) coated magnetic nanoparticles (MNPs). The magnetic nanocomposites were characterized by X-ray powder diffraction (XRD), Fourier transform infrared spectroscopy (FT-IR), thermogravimetry analysis (TGA), vibrating sample magnetometer (VSM), and scanning electron microscopy (SEM). The XRD results showed that the MNPs and nanocomposite are pure magnetite. The FTIR analysis confirmed the binding of CS on the surface of the MNPs and also the loading of Nyst in the nanocomposite. The Nyst drug loading was estimated using UV-Vis instrumentation and showing a 14.9% loading in the nanocomposite. The TEM size image of the MNPs, CS-MNP, and Nyst-CS-MNP was 13, 11, and 8 nm, respectively. The release profile of the Nyst drug from the nanocomposite followed a pseudo-second-order kinetic model. The antimicrobial activity of the as-synthesized Nyst and Nyst-CS-MNP nanocomposite was evaluated using an agar diffusion method and showed enhanced antifungal activity against *Candida albicans*. In this manner, this study introduces a novel nanocomposite that can decrease fungus activity on-demand for numerous medical applications.

## 1. Introduction

Recently, advances in nanobiotechnology have led to the preparation of iron oxide nanoparticles with specific sizes and shapes which have the potential to be used as new antimicrobial agents [1–3]. The functional activities of iron oxide nanoparticles are influenced largely by their size. Undoubtedly, iron oxide nanoparticles have numerous applications in medicine due to their magnetic, physical, chemical,

and effective biological properties. Moreover, nanoparticles with smaller particle sizes have been shown to possess antimicrobial properties [4]. The antimicrobial activity of iron oxide nanoparticles has largely been studied against different organisms [1, 5–7] and has been shown to depend on three factors: size, stability, and concentration in the growth medium. The size of microbial cells is in the micrometer range while outer cellular membranes have pores in the nanometer range. Due to the smaller size of nanoparticles

compared to bacterial pores, they have the unique ability of crossing cell membranes. The most common methods to prepare iron oxide nanoparticles are coprecipitation [8], thermal decomposition, hydrothermal [9], polyol methods [10], electrochemical methods [11], and sonication [8].

Stabilization of magnetic nanoparticles can occur by controlling on one or both of the two repulsive forces: electrostatic and steric repulsion [12]. The steric effect depends on the molecular weight and density of the polymers [13, 14], whereas the electrostatic repulsion depends on the ionic strength and pH of the solution. Therefore, playing on these stabilization factors of magnetic particles can be achieved by using different stabilizers; for example, monomeric stabilizers such as carboxylates [15, 16], phosphates [17], inorganic materials such as silica [18], gold [19], polymers stabilizers such as dextran [20], polyethylene glycol [21], polyvinyl alcohol [22], alginate [23], chitosan [24], poly(N-2-hydroxyethyl)-D,L-aspartamide-graft-poly(butyl methacrylate) [25], and folic acid-functionalized composite copolymers [26].

Different researchers studied the diameter stability of magnetic nanoparticles and degradation stability by using dynamic light scattering (DLS) [27] and inductively coupled plasma (ICP) [28]. Yoonjee Park and his research group showed that the effective diameter for citric acid-coated/PEGylated iron oxide nanoparticles did not increase at pH 7 or 9 after 30 days but increased at pH 11 [27]. Similarly Hoskins showed that magnetic nanoparticles coated with poly ethylenimine and poly ethylene glycol were stable at neutral pH and at an acidic environment at a pH of 4.6 in the presence of sodium citrate [28].

Systemic and topical fungal diseases are serious human infections especially in immunocompromised and cancer patients. The increasing resistance of pathogenic fungi urges the modification of currently used antifungal antibiotics. Except for their solubilization, toxicity, and side effect disadvantages, polyene macrolide antibiotic antifungal agents are one of the most effective fungicidal agents [29]. Specifically, Nystatin (21E, 23E, 25E, 27E, 31E, 33E)-20-{[(3S, 4S, 5S, 6R)-4-amino-3,5-dihydroxy-6-methyloxan-2-yl]oxy}-4,6,8,11,12, 16,18,36-octahydroxy-35,37,38-trimethyl-2,14-dioxo-1 oxa cyclo octatriaconta-21, 23, 25, 27, 31, 33-hexaene-17-carboxylic acid is a polyene antifungal antibiotic of broad spectrum antifungal activity [30]. It is possible to decrease the toxicity and harmful side effects of nystatin through its incorporation into iron oxide nanoparticles. In addition, the use of nystatin and iron oxide nanoparticle composites could allow for magnetically directed antifungal therapy.

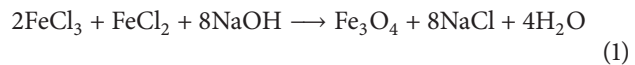
For all of the above reasons, the objectives of this study were for the first time to prepare a nystatin-iron oxide nanocomposite, characterize their structural and magnetic properties, and evaluate their antimicrobial activity by comparison to free nystatin.

## 2. Materials and Methods

**2.1. Materials.** Ferric chloride ( $\text{FeCl}_3 \cdot 6\text{H}_2\text{O}$ ), ferrous chloride ( $\text{FeCl}_2 \cdot 4\text{H}_2\text{O}$ ), and sodium hydroxide were all of analytic grade obtained from Merck KGaA (Darmstadt, Germany).

Chitosan with a deacetylation degree (DD) of 75%–85% and Nystatin (>98% purity; mol.wt 926.1 g/mol) were purchased from Sigma-Aldrich (Saint Louis, MO, USA) and used without any pretreatment. An acetic acid solution at 99.8% was purchased from Hamburg Industries Inc. (Hamburg, Germany). Deionized water was used for all the experiments.

**2.2. Preparation of Magnetic Nanoparticles (MNPs).** The MNPs were prepared by a coprecipitation method according to the literature [8]. The MNPs were prepared by mixing a solution of  $\text{Fe}^{2+}$  (0.3 Mol) and  $\text{Fe}^{3+}$  (0.15 Mol) in a 30 mL aqueous medium. The mixture solutions of Fe ions were added to a 100 mL solution of NaOH (2 Mol); the pH value of the solution was kept above 11. The precipitates of MNPs were produced according to the reaction as follows:



The solution was sonicated for 60 minutes at room temperature. Finally, the precipitate was collected by centrifuge separation (30000 rpm for 20 min at 25°C) and was separately washed three times with deionized water.

**2.3. Preparation of CS-MNP Nanoparticles.** The CS solution was prepared by dissolving 0.5 g of CS powder in a 1% acetic acid solution. CS-MNP nanoparticles were prepared by mixing CS with a suspension of  $\text{Fe}_3\text{O}_4$  nanoparticles. After the mixture was stirred and mixed completely during 18 hours, the coated particles were separated by a permanent magnet and were dried at the 70°C for two hours. The product was denoted as CS-MNP (chitosan coated magnetic nanoparticles).

**2.4. Preparation of Nyst-CS-MNP Nanocomposite.** The solution of Nyst was prepared by dissolving 0.86 g into acetone. The Nyst-CS-MNP nanocomposite was prepared by mixing a solution of Nyst (5 mg/mL) with a known weight of each CS-MNP nanoparticle (40 mg/mL). The solution was magnetically stirred at room temperature for 18 hours to facilitate Nyst uptake. The products were separated by the use of a permanent magnet and were denoted as Nyst-CS-MNP (loaded kojic acid on the chitosan coated magnetic nanoparticles).

**2.5. Loading and Release of Nystatin from the Nyst-CS-MNP Nanocomposite.** Nystatin release profiles from the nanocomposite were determined at room temperature using a phosphate buffered saline solution (PBS) at a concentration of 0.01 mol/L at pH 7.4. About 85 mg of the nanocomposite was added to 500 mL of the PBS media. The release medium (3 mL) was removed for analysis at given time intervals at  $\lambda_{\max} = 290$  nm using a Perkin Elmer UV-Vis spectrophotometer, model Lambda 35, and replaced with 3 mL of the buffered solution. The cumulative amount of Nystatin released into the solution was measured at preset time intervals.

To compare the release rate of Nystatin from the Nyst-CS-MNP nanocomposite, with the physical mixture which

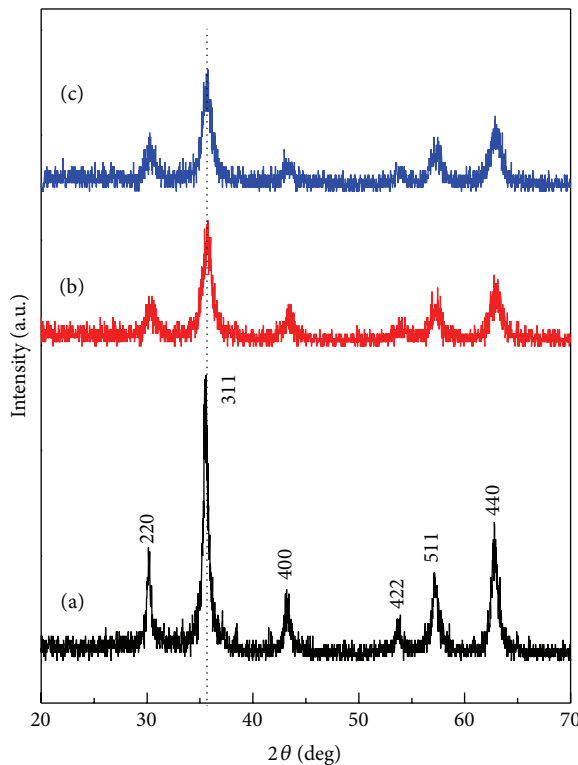


FIGURE 1: X-ray powder diffraction patterns of the MNPs (a), CS-MNP (b), and the Nyst-CS-MNP nanocomposite (c).

contained Nystatin with polymers and MNPs, 3.0 mg of the physical mixture was obtained by mixing 0.40 mg of nystatin with 0.06 mg of CS and 2.50 mg of MNPs nanoparticles. The release of the active nystatin was determined as described above.

## 2.6. Antimicrobial Activity Tests

**2.6.1. Effect of Nys-CS-MNP on Microbial Growth.** In order to quantitatively evaluate the effect of the as-synthesized Strep-CS-MNP on the growth kinetics of different microorganisms, the plate colony counting method was employed as described previously [31]. In brief, prior to treatment with the Nys-CS-MNP, the microbial cultures of *Staphylococcus aureus* (ATCC 43300), *Pseudomonas aeruginosa* (ATCC 27853), *Escherichia coli* (ATCC 25922), and *Candida albicans* (ATCC 20408) were obtained from the American Type Culture Collection (ATCC, Manassas, VA, USA) and were hydrated and streaked for isolation on tryptic soy agar plates. Following growth, a single isolated colony was selected and used to inoculate 3 mL of 20% tryptic soy broth (TSB) medium. The bacterial culture was grown on a shaking incubator set at 200 rpm for 18 hours at 37°C. The resulting bacterial suspension was then adjusted to have an OD<sub>570</sub> of 0.52, corresponding to a bacterial density of 10<sup>9</sup> colony forming units (CFU) per mL. Then, the bacterial suspension was serially diluted over a 4-log range to a bacterial density of 10<sup>4</sup> CFU/mL using 20% TSB. A volume of 1 mL of the bacterial suspension was

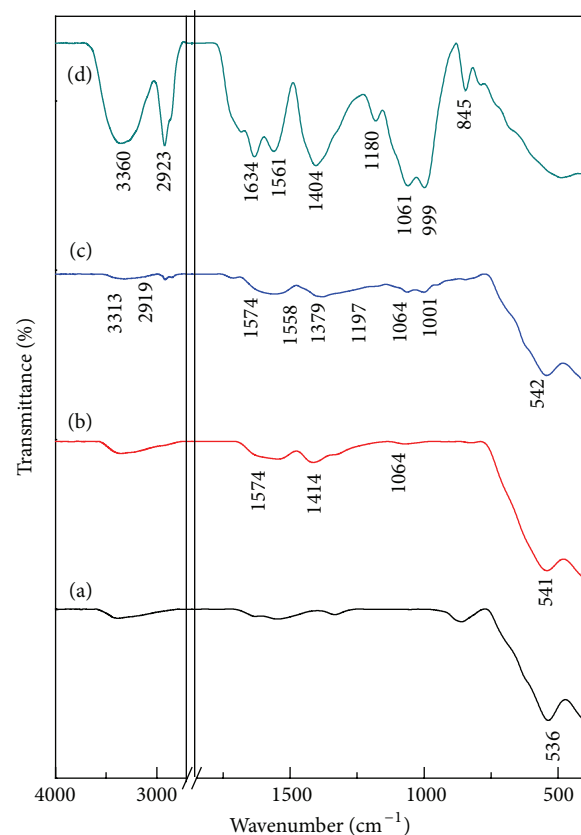


FIGURE 2: FTIR spectra of MNPs (a), CS-MNP (b), Nyst-CS-MNP (c), and free Nyst (d).

treated with the nanocomposite suspension at concentrations of 10 and 20 mg/mL in a separate well of a 24-well plate and allowed to incubate for 1 hr at 37°C. The number of CFU after treatment was determined using the plate counting method following plating on tryptic soy agar plates. The experiment was repeated in triplicate. The percentage of inhibition of the nanocomposite against each microorganism was calculated according to the following equation:

$$\text{Inhibition rate} = 1 - \left[ \frac{\text{OD}_{\text{treated}}}{\text{OD}_{\text{control}}} \right] \times 100. \quad (2)$$

The efficiency of the nanoparticles to inhibit the growth of microorganisms was determined by calculating differences in the equivalent number of colony forming units before and after treatment as a percentage of microbes that were inhibited by the particles and was calculated from the previous equation.

**2.6.2. Agar Diffusion Susceptibility Test and Determination of Minimum Inhibitory Concentrations.** Prior to incubation with nanoparticles, the yeast strain was cultured overnight in 5 mL of potato dextrose broth (Difco, USA) in a Certomat BS-T incubation shaker (Sartorius Stedim Biotech, Aubagne, France) at 37°C, 150 rpm until the culture reached an OD<sub>600</sub> of 1.0 (Spekol UV-Vis 3.02, Analytic Jena, Jena, Germany), corresponding to 10<sup>9</sup> CFU·mL<sup>-1</sup>. The overnight

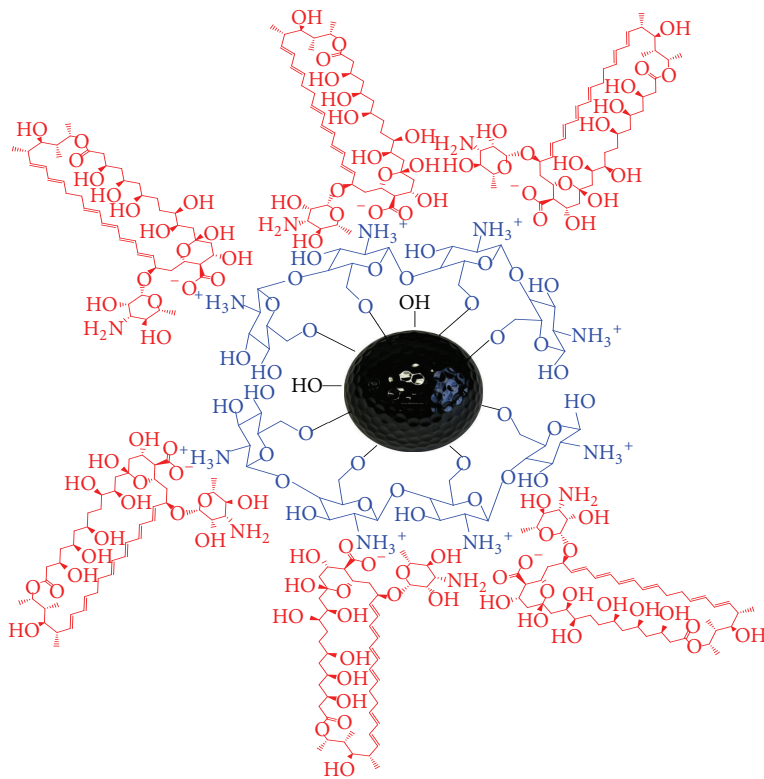


FIGURE 3: Scheme representing the interaction between Nyst, CS, and MNPs in the Nyst-CS-MNP nanocomposite.

cultures were diluted to  $10^8 \text{ CFU} \cdot \text{mL}^{-1}$  using sterile broth. The antimicrobial activity of the as-synthesized Nystatin nanoparticles (Nyst-CS-MNP nanocomposite) was evaluated against *Candida albicans* using both disc and cup agar diffusion methods as described previously [32]. The Nyst-CS-MNP nanocomposites (100 mg) were suspended in 1 mL of sterilized phosphate buffered saline and the discs were soaked in the suspension. The loaded discs were applied on the surface of the seeded agar plates using sterile forceps. The diameters of the zones of inhibition were measured after 24 hours of incubation at  $37^\circ\text{C}$ . The experiment was repeated in triplicate and an average of the zones of inhibition was determined. Free Nystatin (100 mg/mL) was used as a control. MNPs and CS-MNP were also tested for any possible antimicrobial activity using the same method.

In order to determine the MIC values of the nanocomposite against different microorganisms, a broth microdilution method was employed. The bacterial suspensions were prepared as described above. The MIC were determined over a range of 2000 and  $10 \mu\text{g}/\text{mL}$  by a twofold serial dilution method.

**2.7. Cell Culture.** Normal mouse fibroblast cells (3T3) were obtained from the American Type Culture Collection (ATCC, Manassas, VA, USA). The cells were maintained and cultured in DMEM medium with 10% fetal bovine serum (FBS), 15 mmol/L L-glutamine, 100 units/mL penicillin, and  $100 \mu\text{g}/\text{mL}$  streptomycin to maintain cells at  $37^\circ\text{C}$  and 5%  $\text{CO}_2$  in a humidified incubator. Media were changed every two

days and at 90% confluent, cells were seeded into 96-well plates at  $1 \times 10^5$  cells/mL and kept overnight for cell attachment. We discarded the old media and added  $100 \mu\text{L}$  of new media containing pure nystatin and magnetic nanoparticles were used to treat the cells, while wells containing media and cells only were used as controls. For each experiment a freshly prepared stock solution of Nyst, MNPs, CS-MNP, and Nyst-CS-MNP was used for the treatment. A stock of  $10 \text{ mg/mL}$  (in PBS) was made, and DMEM medium was used to obtain the desired concentration required for the treatment through serial dilution ( $0\text{--}100 \mu\text{g}/\text{mL}$ ). The MTT assay was used 72 hours after exposure to determine the toxic effect of these agents.

**2.8. MTT Assay.** In this assay, the MTT reagent (3,(4,5-dimethylthiazol-2-yl)-2,5-diphenyltetrazolium bromide) is converted into an insoluble and brightly coloured formazan when added to cells in culture. The reaction takes two-four hours for completion and it depends on the conversion of the MTT reagent by only viable cells. The MTT assay was conducted as described previously [33]. In brief the treatment media was discarded after 72 hours and the MTT containing media was added at  $5 \text{ mg/mL}$  PBS to a volume of  $100 \mu\text{L}$  per well and the plates were incubated at  $37^\circ\text{C}$  in a 5%  $\text{CO}_2$  humidified incubator. After a two hour period, the detergent Dimethyl sulfoxide (DMSO) was then added to the cells to stop the conversion and solubilize the formazan. The amount of formazan correlates directly with the number of viable cells after treatment. Absorbance of the formed formazan was

taken at a wavelength of 570 nm using a multiwall microplate reader. Experiments were made in triplicate and results were expressed as mean  $\pm$  SD

$$\text{cell viability (\%)} = \frac{\text{Average of treated}}{\text{average control}} \times 100\%. \quad (3)$$

**2.9. Instrumentation.** Powder X-ray diffraction patterns were used to determine the crystal structure of the samples in the range of 25–70 degrees on an XRD-6000 diffractometer (Shimadzu, Tokyo, Japan) using CuK $\alpha$  radiation ( $\lambda$  1.5406 Å) at 30 kV and 30 mA. Fourier transform infrared spectroscopy (FTIR) spectra of the materials were recorded over the range of 400–4000 cm $^{-1}$  on a Thermo Nicolet Nexus, Smart Orbit spectrometer using the KBr disc method. Thermogravimetric analysis was carried out using a Metter-Toledo 851e instrument (Switzerland) with a heating rate of 10°C/min, in 150  $\mu$ L alumina crucibles and in the range of 30°C–900°C. Scanning electron microscopy was used to observe the surface morphology of the samples using a NOVA NanoSEM 230 (FEI, Hillsboro, OR) scanning electron microscope. Magnetic properties were evaluated by a Lakeshore 7404 vibrating sample magnetometer (VSM). The zeta potential was measured at 25°C by dynamic light scattering (DLS), using a Malvern Zetasizer Nano ZS (Malvern Instruments, Malvern, UK). The mean particle size of the samples was obtained using a transmission electron microscope (Hitachi H-7100, Tokyo, Japan) at an accelerating voltage of 80 and 200 kV. UV-Vis spectra were measured to determine the optical properties and a controlled release study, using an ultraviolet-visible spectrophotometer (Perkin Elmer, Waltham, MA).

**2.10. Statistical Analysis.** Statistical analysis was used to compare the percentage inhibition of Nyst and nanocomposites against different microorganisms using a two-way ANOVA test. The Prism V6.01 statistical software (GraphPad, San Diego, CA, USA) was used for data management and statistical analysis. All data are shown as the mean  $\pm$  standard deviation unless indicated differently.

### 3. Results and Discussion

**3.1. X-Ray Diffraction (XRD).** Figure 1(a)–1(c) show the XRD patterns for the MNPs, the CS-MNP coated, and the Nyst-CS-MNP nanocomposite, respectively. All six diffraction peaks at  $2\theta = 30.2^\circ, 35.5^\circ, 43.2^\circ, 53.5^\circ, 57.2^\circ$ , and  $62.7^\circ$  were indexed to the (2 2 0), (3 1 1), (4 0 0), (4 2 2), (5 1 1), and (4 4 0) planes, respectively, which are related to the cubic spinel phase of Fe<sub>3</sub>O<sub>4</sub> [4, 34]. The peak positions of MNPs nanoparticles are unchanged between Figures 1(b) and 1(c), which illustrated that the binding process did not result in a phase change of the MNPs. The peak intensity of the Nyst-CS-MNP nanocomposite is lower than that of the CS-coated MNPs and MNPs which may due to the fact that the MNPs are incorporated with Nyst drugs.

The average particle sizes can be quantitatively evaluated from the XRD data using the Debye-Scherrer equation, which

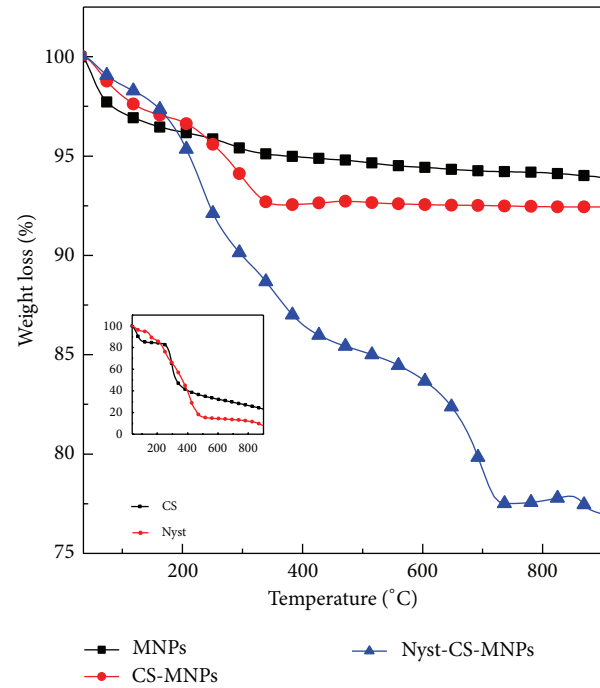


FIGURE 4: TGA analysis curves of MNPs, CS-MNP, and Nyst-CS-MNP; the inset shows the TGA curve of pure CS and Nyst.

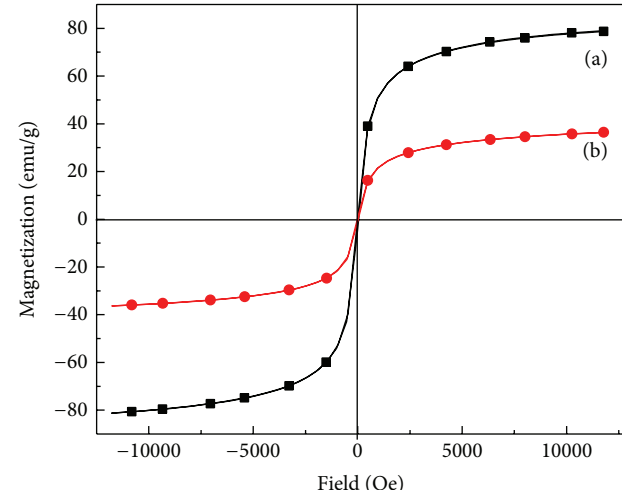


FIGURE 5: Magnetization curves obtained by vibrating sample magnetometer (VSM) at room temperature: (a) MNPs and (b) the Nyst-CS-MNP nanocomposite.

gives a relationship between peak broadening in XRD and average particle sizes (4):

$$D = \frac{k\lambda}{\beta \cos \theta}, \quad (4)$$

where  $D$  is the mean grain size,  $k$  is the Scherrer constant (0.89),  $\lambda$  is the wavelength of the X-ray diffraction (0.15418 nm),  $\theta$  is the Bragg diffraction angle in degree, and  $\beta$  in radian is the full width at half maximum intensity. The diffraction peak which corresponds to the lattice

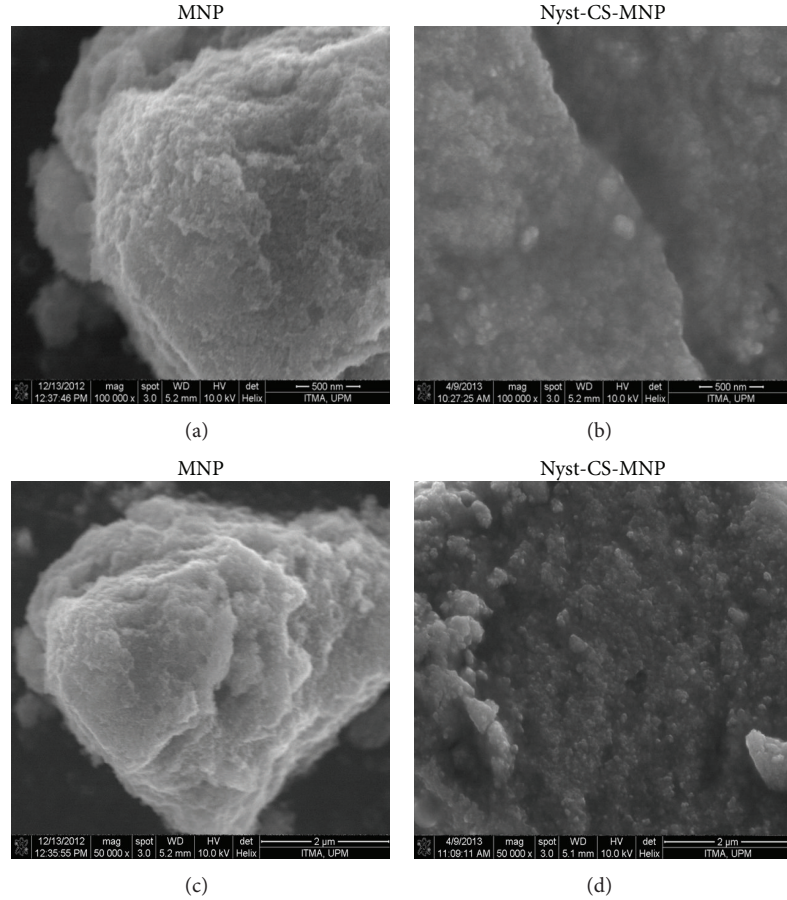


FIGURE 6: SEM images of MNPs and Nyst-CS-MNP.

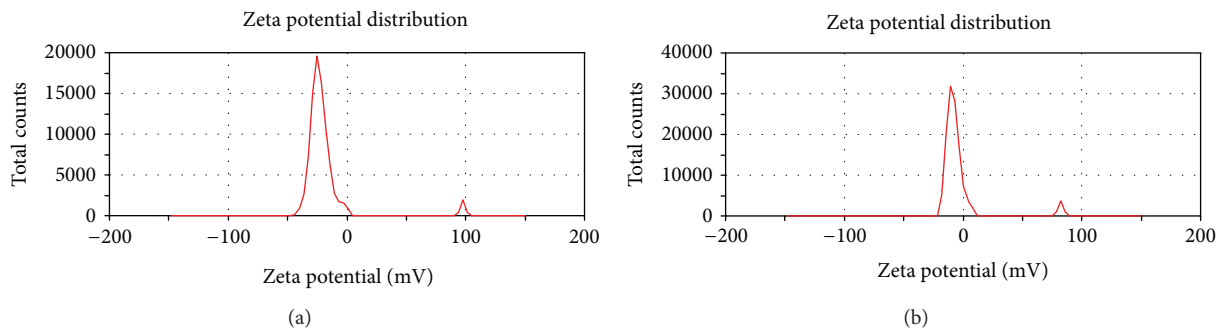


FIGURE 7: Zeta potential measurements of MNPs (a) and the Nyst-CS-MNP nanocomposite (b).

plane (311) at  $2\theta = 35.4^\circ$  was used for calculation because this peak is well resolved and does not show any interferences. The average particle sizes of the MNPs, CS-coated MNPs, and Nyst-CS-MNP nanocomposite obtained from this equation were found to be about 39.5, 27.0, and 15.5 nm, respectively.

**3.2. Infrared Spectroscopy (FTIR).** The FT-IR spectra of MNPs, CS-coated MNPs, Nyst-CS-MNP nanocomposite, and free Nyst are shown in Figure 2. In the spectra of the

MNPs (Figure 2(a)), the absorption peak at  $536\text{ cm}^{-1}$  is characteristic of Fe-O-Fe in  $\text{Fe}_3\text{O}_4$ . However, this characteristic peak of Fe-O-Fe shifts to 541 and  $542\text{ cm}^{-1}$  for CS-coated MNPs nanoparticles and Nyst-CS-MNP nanocomposites, respectively. This result confirms the presence of magnetite nanoparticles.

For the IR spectrum of CS-coated MNPs nanoparticles (Figure 2(b)), the FTIR of CS-coated MNPs nanoparticles showed the characteristic peaks of CS, proving that magnetite nanoparticles were successfully coated with chitosan. For example, a peak around  $1574\text{ cm}^{-1}$  assigned to  $\text{NH}_3^+$  was

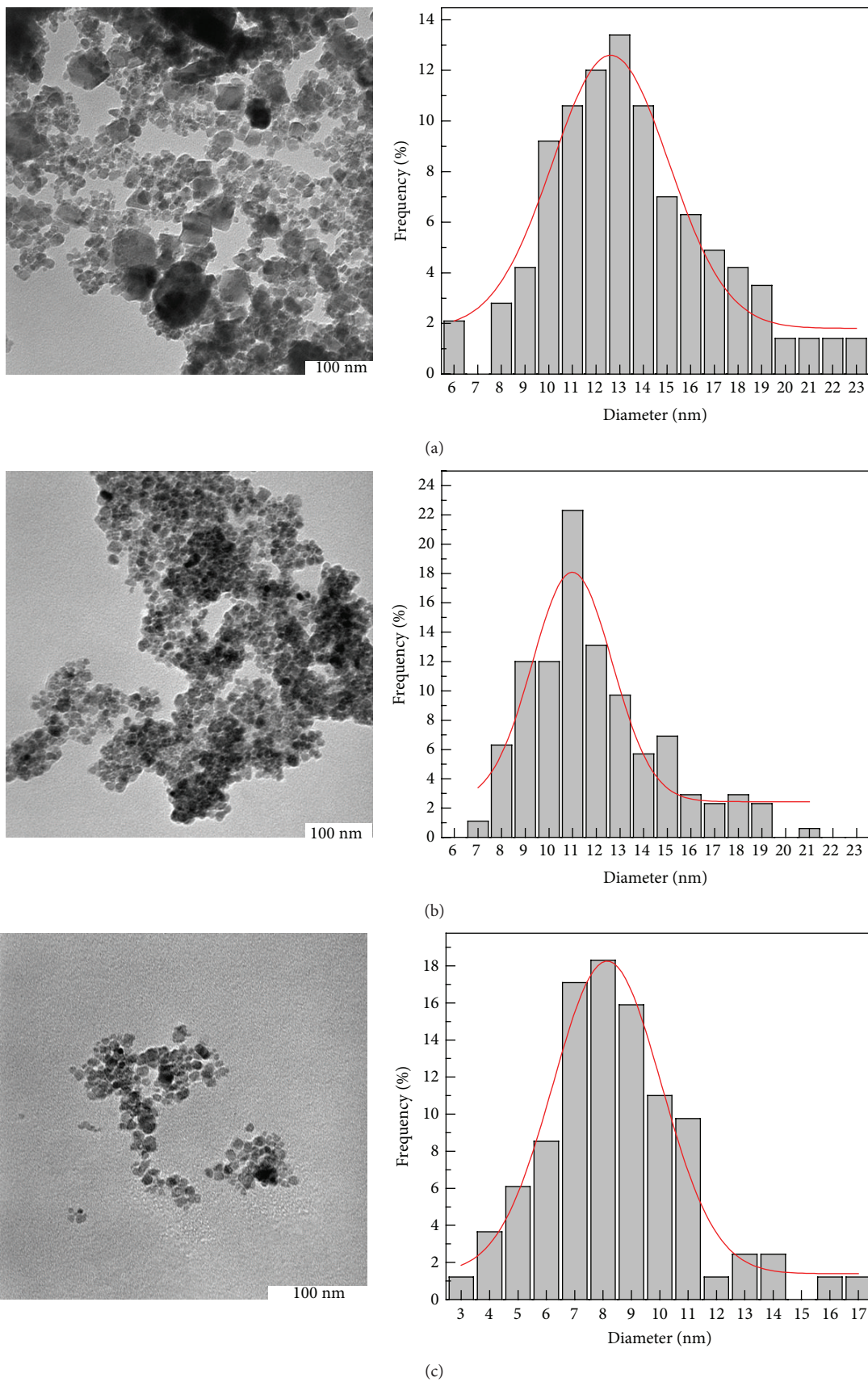


FIGURE 8: Transmission electron micrographs and particle size distribution for MNPs (a), CS-MNP nanoparticles (b), and Nyst-CS-MNP nanocomposite (c).

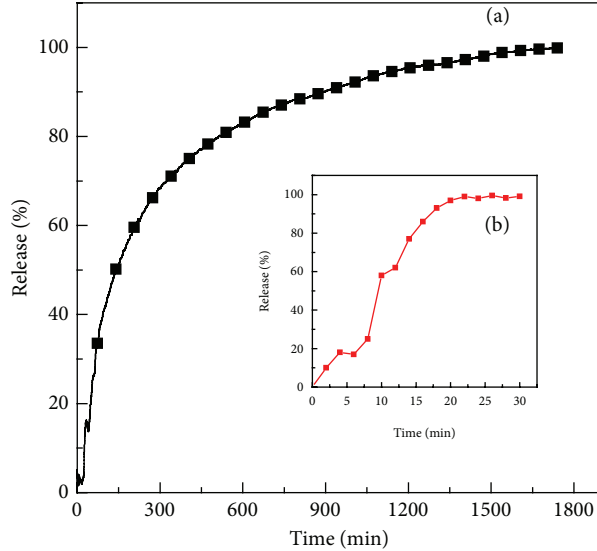


FIGURE 9: Release profiles of nystatin from the Nyst-CS-MNP nanocomposite at a pH of 7.4 (a). Inset shows the release profiles of nystatin from the physical mixture (b).

identified [35]. In addition, the glycosidic bond stretching vibrations between the MNPs and CS appeared at  $1064\text{ cm}^{-1}$  [33].

For the IR spectrum of the Nyst-CS-MNP nanocomposite (Figure 2(c)), the appearance of Nyst peaks in the Nyst-CS-MNP nanocomposites confirmed the loading of Nyst drugs on the surface of the CS-MNP nanoparticles. The absorption peaks at  $1558$  and  $1379\text{ cm}^{-1}$  could be assigned to asymmetric and symmetric stretching vibrations of  $\text{COO}^-$  anion groups. These results indicate that the carboxylic groups of Nyst are dissociated into  $\text{COO}^-$  groups which complex with protonated amino groups of chitosan through electrostatic interactions to form the polyelectrolyte complex during the polymerization procedure (Figure 3) [36].

**3.3. Thermogravimetric Analysis (TGA).** Figure 4 shows the TGA curves of MNPs, CS-coated MNPs nanoparticles, and the Nyst-CS-MNP nanocomposite. The TGA curve of MNPs shows that the weight loss over the temperature range from  $35^\circ\text{C}$  to  $850^\circ\text{C}$  was about 5.8%. This might be due to the loss of residual water in the sample.

The TGA curves of the CS-coated MNPs provide indications of the content of the CS polymers. The CS polymer began to degrade at about  $250^\circ\text{C}$  (inset for Figure 4) and the final temperature of decomposition was around  $850^\circ\text{C}$ , with a total weight loss 7.7%. This result indicates that the average mass content of CS in CS-MNP nanoparticles was about 1.9%. On the other hand, for the Nyst-CS-MNP nanocomposites, below  $200^\circ\text{C}$ , the weight loss of the nanocomposite was quite small (2%) because of the removal of the absorbed physical and chemical water. Then, the principle chains of the Nyst-CS began to degrade at about  $200^\circ\text{C}$  and the temperature of the final decomposition was around  $817^\circ\text{C}$ ; the weight loss was significant (21%). The weight loss at CS-coated MNPs

nanoparticles was lower than that for the Nyst-CS-MNP nanocomposite; this result confirmed the loaded Nyst drug at the surface of the CS-MNP nanoparticles.

The loading amount of Nyst in the Nyst-CS-MNP nanocomposite was estimated using a UV-visible spectrophotometer and a standard curve of a series of standard solutions of known Nyst concentrations. The UV-visible spectrophotometer showed that the Nyst loaded was 14.9%.

**3.4. Measurements of Magnetic Properties.** Figures 5(a) and 5(b) show the VSM of the MNPs nanoparticles and the Nyst-CS-MNP nanocomposite, respectively. As shown in Figure 5, the magnetization of the samples approached the saturation values when the applied magnetic field increased to 11,780 Oe. The saturation magnetization of the MNPs was 78.7 emu/g. For the Nyst-CS-MNP nanocomposite, the saturation magnetization was about 36.4 emu/g. The saturation magnetization of the nanoparticles was much less than that of the bulk magnetite, which was 84 emu/g [37]. The lower value of the measured saturation magnetization was due to the smaller size of magnetite and the lower saturation magnetization of the Nyst-CS-MNP nanocomposite which may be attributed in a larger part to the incorporation of MNPs nanoparticles into Nyst-CS which added mass of the thick polymer layer on the magnetite nanoparticles. When the magnetic component size of the particles is smaller than the critical size, the particles will exhibit superparamagnetism.

**3.5. Scanning Electron Microscopy (SEM).** Figures 6(a) and 6(b) show the SEM images of the MNPs and Nyst-CS-MNP nanocomposite at 100,000x magnification and Figures 6(c) and 6(d) show the SEM images of the MNPs and Nyst-CS-MNP nanocomposite at 50,000x magnification. Figures 6(a) and 6(c) show a very strong agglomeration which is due to

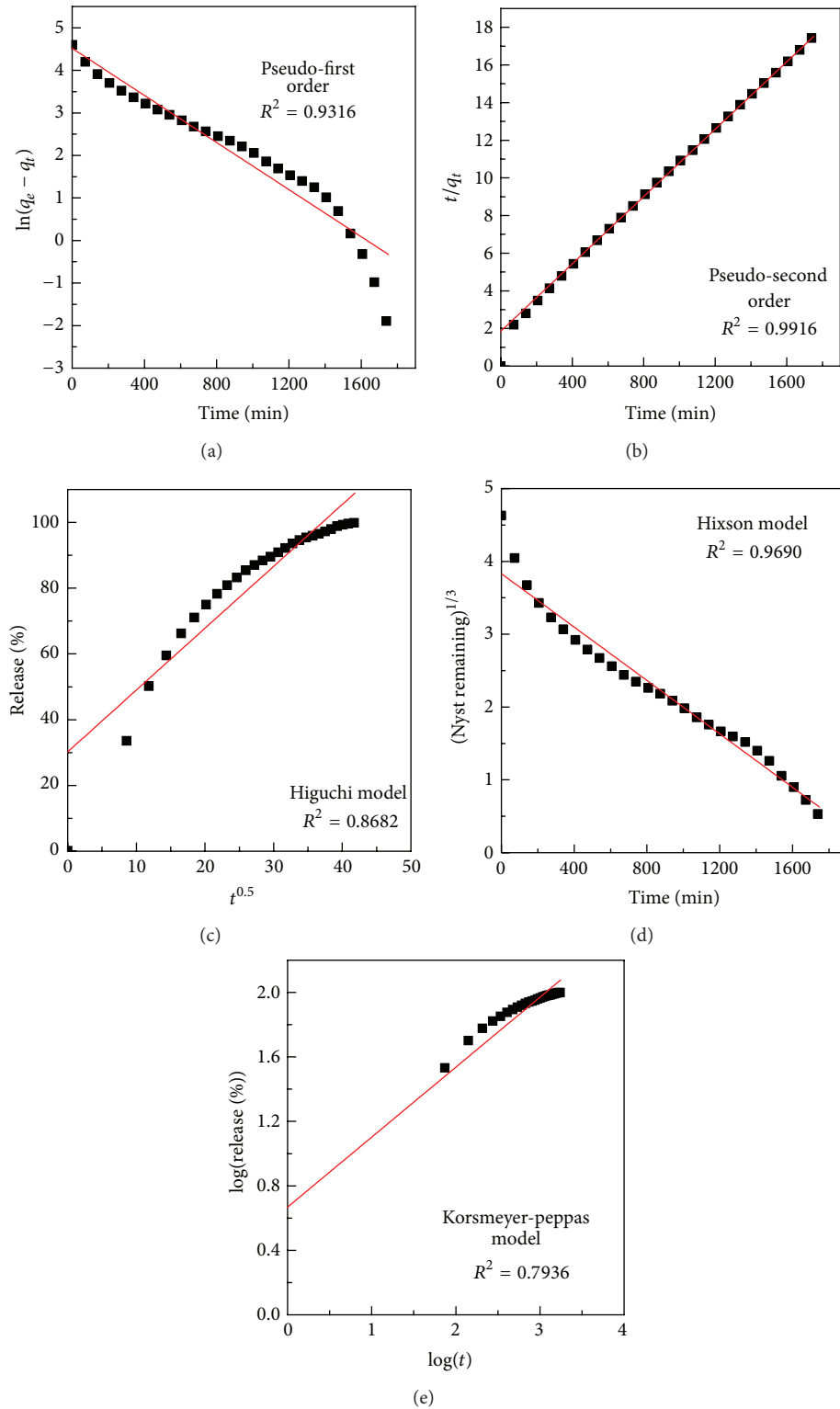


FIGURE 10: Fitting of the data about Nyst release from the Nyst-CS-MNP nanocomposite for different kinetic models at a pH of 7.4.

the Van der Waals force between the particles. The degree of agglomeration decreased after coating the nanoparticle with the CS polymer to get the Nyst-CS-MNP nanocomposite (Figures 6(b) and 6(d)).

**3.6. Determination of Zeta Potential and Particles Size Distribution.** Figures 7(a) and 7(b) show the zeta potential measurement of the MNPs and Nyst-CS-MNP nanocomposite, respectively, suspended in deionized water. The zeta potential

TABLE 1: Correlation coefficients ( $R^2$ ) obtained by fitting the Nyst release data from the Nyst-CS-MNP nanocomposite into PBS solutions at pH 7.4.

Samples	Saturation release (%)	Pseudo-first order	Pseudo-second order	Higuchi model	Hixson-Crowell model	Korsmeyer-Peppas model
Nyst-CS-MNP	100	0.9316	0.9916	0.8682	0.9690	0.7936

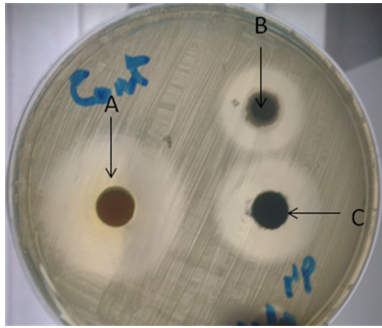


FIGURE 11: The zones of inhibition of free nystatin (A) as a control and the Nyst-CS-MNP nanocomposite ((B), disc-loaded nanoparticles and (C), water-suspended nanoparticles in a cup) against *Candida albicans* using the agar diffusion method. MNPs and CS-MNP did not show any zone of inhibition when tested similarly.

is about  $-19.4$  mV that provides electrostatic repulsion forces between nanoparticles. The zeta potential of the Nyst-CS-MNP nanocomposite had a less negative value compared to MNPs with a  $-2$  mV value; this result was similar to the literature [38].

The TEM image of the MNPs was spherically shaped, with a size of 6 nm to 23 nm showing a mode value of 13 nm (Figure 8(a)). After coating MNPs with chitosan (Figure 8(b)), the dispersibility of the MNPs increased significantly, which is useful in biomedical applications. As can be seen in Figure 8(b), the CS-MNP were almost spherical in shape and with average sizes of 11 nm. After loading nystatin (Figure 8(c)), there was no apparent difference between the CS-MNP and Nyst-CS-MNP nanocomposite; the latter also shows a spherical shape with average sizes of 8 nm. The decreasing average particle sizes for CS-coated MNPs and Nyst-CS-MNP nanocomposites compared to MNPs may be attributed to the prolonged vigorous stirring at high speeds after the addition of the polymer and the drugs. A similar result was reported by Yu and Chow [39].

**3.7. In Vitro Release of Nyst from the Nyst-CS-MNP Nanocomposite.** The release profiles of Nystatin from the Nyst-CS-MNP nanocomposite and the physical mixture of Nystatin, CS, and MNPs are shown in Figures 9(a) and 9(b), respectively. The physical mixture of Nystatin, CS, and MNPs exposed to pH 7.4 environments showed the release of Nystatin very quickly, within 20 minutes (Figure 9(b)). In contrast, the release rate of Nystatin from the Nyst-CS-MNP nanocomposite was slower than from the physical

mixture, indicating that the nanocomposite has the potential to be used for the controlled release of antimicrobial agents. This result may be attributed to the interaction between the negatively charged Nystatin and the positively charged protonated chitosan.

In Figure 9(a), the percent release of Nystatin from the Nyst-CS-MNP nanocomposite reached about 100% within about 1800 minutes. The release mechanism would occur primarily through the ion exchange between the Nystatin and the negative anions available in the PBS.

**3.8. Release Kinetics of Nyst from Nysts-CS-MNP Nanocomposite.** To analyze the in vitro release data of Nyst from the Nyst-CS-MNP nanocomposite, various kinetic models were used to describe the release kinetics, for example, pseudo-first-order model (5) [40], pseudo-second-order model (6) [41], Higuchi model (7) [42], Hixson-Crowell model (8) [43], and the Korsmeyer-Peppas model (9) [44]:

$$\ln (q_e - q_t) = \ln q_e - kt \quad (5)$$

$$\frac{t}{q_t} = \frac{1}{k} q_e^2 + \frac{t}{q_e} \quad (6)$$

$$q_t = K \sqrt{t} \quad (7)$$

$$\sqrt[3]{M_o} - \sqrt[3]{M_t} = Kt \quad (8)$$

$$\frac{q_t}{q_\infty} = Kt^n, \quad (9)$$

where  $q_e$  and  $q_t$  are the equilibrium release amounts and the release amount at any time ( $t$ ), respectively,  $M_o$  and  $M_t$  are the initial amounts and the amount of the drug in the nanocomposite at time  $t$ , respectively.

Using the five kinetic models in the release kinetic data of Nyst, in the pseudo-first order (Figure 10(a)), the  $R^2$  value obtained was 0.9316 and more satisfactory for describing the release kinetic processes of Nyst from the Nyst-CS-MNP nanocomposite was the pseudo-second order (Figure 10(b)) with  $R^2 = 0.9916$ . The Higuchi's equation plot (Figure 8(c)) ( $R^2 = 0.8682$ ) indicated the release of the drug from the matrix as a square root of time in-dependent process based on Fickian diffusion. The dissolution data was also plotted in accordance with the Hixson Crowell cube root law (Figure 10(d)) with an  $R^2 = 0.9690$  value. Finally, the Korsmeyer-Peppas model gave an  $R^2$  value of 0.7936. The resulting correlation coefficient values are listed in Table 1.

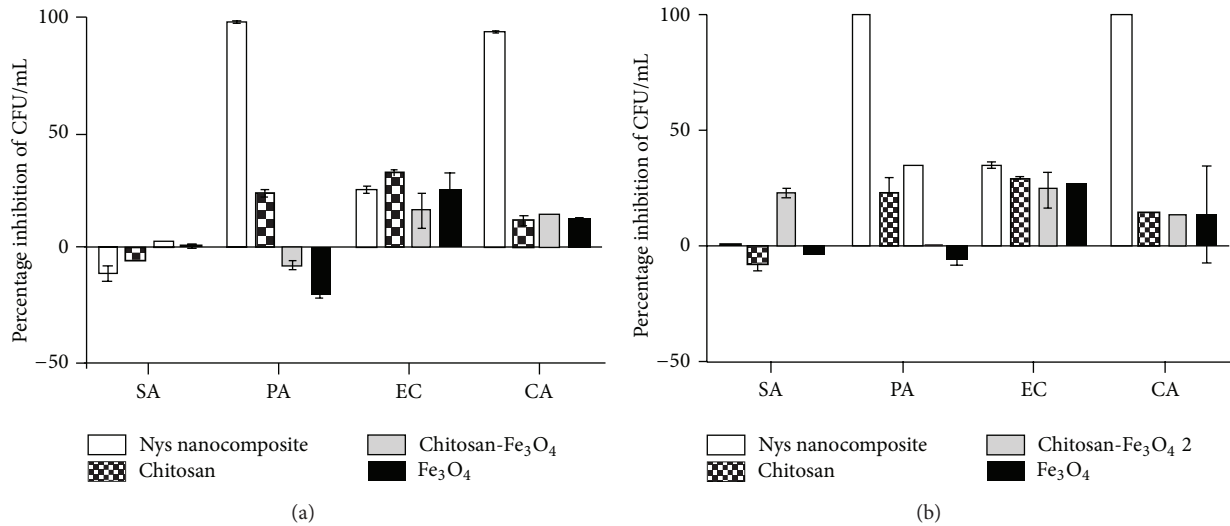


FIGURE 12: Growth inhibition of nystatin chitosan magnetic nanocomposite against different microorganisms using the plate colony counting method at two concentrations ((a): 1 mg) and ((b): 2 mg). Abbreviations: CFU, colony-forming units; SA: *Staphylococcus aureus*; PA: *Pseudomonas aeruginosa*; EC: *E. coli*; and CA: *Candida albicans*.

TABLE 2: Percentage inhibition of nystatin chitosan magnetic nanocomposite against different microorganisms.

Sample	Concentration	<i>Staphylococcus aureus</i>	Percentage inhibition (Mean ± SEM)		
			<i>Pseudomonas aeruginosa</i>	<i>Escherichia coli</i>	<i>Candida albicans</i>
Nys-CS-MNP	1 mg	-10.236 ± 1.821	99.014 ± 0.081	25.771 ± 0.498	93.750 ± 0.125
Nys-CS-MNP	2 mg	1.312 ± 0.000	99.085 ± 0.000	35.075 ± 0.431	99.957 ± 0.025
CS	1 mg	-4.987 ± 0.000	23.994 ± 0.814	32.313 ± 0.431	11.638 ± 1.246
CS	2 mg	-7.087 ± 1.821	22.535 ± 4.071	28.761 ± 0.431	14.828 ± 0.000
MNPs	1 mg	0.787 ± 0.910	-19.718 ± 0.814	25.373 ± 4.314	13.362 ± 0.249
MNPs	2 mg	-2.887 ± 0.000	-4.676 ± 1.889	26.866 ± 0.000	13.793 ± 12.458
CS-MNP	1 mg	2.887 ± 0.000	-7.042 ± 0.814	16.418 ± 4.314	14.828 ± 0.000
CS-MNP	2 mg	22.835 ± 0.910	1.268 ± 0.081	24.627 ± 4.314	14.267 ± 0.000

**3.9. Antimicrobial Activity of the Nyt-Cs-MNP Nanocomposite.** In the present study, the antimicrobial activity of the Nyst-CS-MNP nanocomposite against *Candida albicans* was determined using the standard agar diffusion and quantitative growth inhibition methods. The Nyst-CS-MNP nanocomposite exhibited high antimicrobial activity against *Candida albicans* by showing a clear inhibition zone as shown in Figure 11 by employing the nanoparticle impregnated disks. The diameters of the inhibition zone of the Nyst-CS-MNP nanocomposite were B; 20 mm, C; 24 mm as compared to 32 mm of free nystatin (A) which indicates that the as-synthesized Nyst-CS-MNP nanocomposite possesses comparable enhanced antifungal activity.

As shown in Figure 12 and Table 2, the Nys-CS-MNP nanocomposite inhibited the growth of different microorganisms at different rates. The Nys-CS-MNP was highly active against *Candida albicans* and *Pseudomonas aeruginosa* and *E. coli*, while it showed poor activity against *Staphylococcus aureus*. The MICs of Nys-CS-MNP against *Staphylococcus aureus*, *Pseudomonas aeruginosa*, *E. coli*, and *Candida albicans* were 5.5, 0.01, 2.7, and 0.667, respectively.

**3.10. MTT Assay.** The effect of free nystatin, MNPs, CS-MNP, and Nyst-CS-MNP nanocomposite on 3T3 cells was assessed by the MTT assay. As shown in Figure 13, no toxic effects on cell viability up to 100 µg/mL could be seen for MNPs, CS-MNP, and Nyst-CS-MNP nanocomposite. The 3T3 cells viability at 100 µg/mL for these samples was 101.6, 88.9, and 64.8%. It is worth mentioning that the viability by using free nystatin at 100 µg/mL was 24.8%.

#### 4. Conclusions

A Nyst-CS-MNP nanocomposite was successfully prepared by coating MNPs nanoparticles with CS and then loading with the Nyst drug. X-ray diffraction analysis showed phase purity of the prepared magnetite nanoparticles as well as the final nanocomposite. Fourier transform infrared spectroscopy showed the vibration modes of the MNP, CS, and Nyst, confirming the coated CS to MNPs and loaded Nyst. Vibrating sample magnetometer studies showed the supermagnetic properties of MNP. The TEM size image of the MNPs, CS-MNP, and Nyst-CS-MNP was 13, 11, and 8 nm,

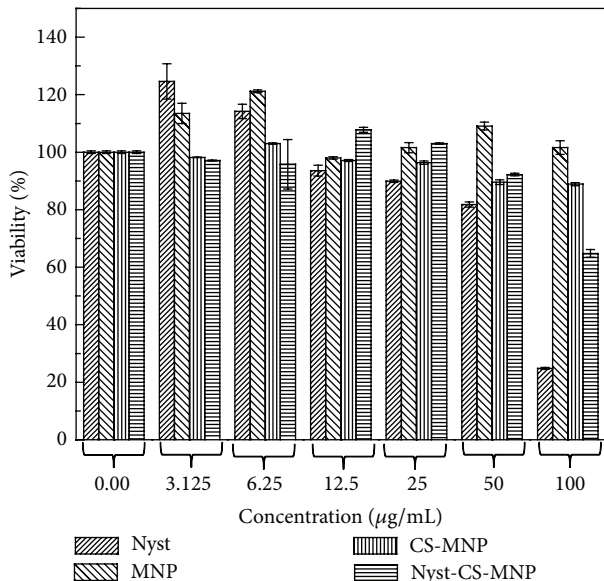


FIGURE 13: MTT assays of a normal fibroblast (3T3) cell line after 72 hours of treatment with free nystatin, MNPs, CS-MNP, and Nyst-CS-MNP at different concentrations.

respectively. The Nyst loading was 14.9%. The drug release was also studied; the total release equilibrium of Nyst from CS-MNP was 100% in 1800 minutes. To our knowledge, this is the first report on the synthesis of a nystatin nanocomposite polyene macrolide nanoantibiotic. These results indicate that as-synthesized the Nyst-CS-MNP nanocomposite can be further used as an antifungal as well as antibacterial agent for human use with less toxicity. However, further *in vivo* studies are required before recommending the use of Nyst-CS-MNP safely in clinical situations to assess the levels of its toxicity.

## Conflict of Interests

The authors declare no conflict of interests in this work.

## Acknowledgments

The authors would like to thank the Ministry of Higher Education of Malaysia under Grant ERGS/1/11/STG/UPM/01/18 (vote 5527050) and the University Putra Malaysia for the postdoctoral support of Samer Hasan Hussein-Al-Ali. The authors would like to thank the Northeastern University, MA, USA, for funding part of the microbiological experiments.

## References

- [1] B. Stephen Inbaraj, T.-Y. Tsai, and B.-H. Chen, "Synthesis, characterization and antibacterial activity of superparamagnetic nanoparticles modified with glycol chitosan," *Science and Technology of Advanced Materials*, vol. 13, no. 1, Article ID 015002, 2012.
- [2] A. Azam, A. S. Ahmed, M. Oves et al., "Antimicrobial activity of metal oxide nanoparticles against gram-positive and gram-negative bacteria: a comparative study," *International Journal of Nanomedicine*, vol. 7, pp. 6003–6009, 2012.
- [3] S. L. Iconaru, A. M. Prodan, P. Le Coustumer et al., "Synthesis and antibacterial and antibiofilm activity of iron oxide glycerol nanoparticles obtained by coprecipitation method," *Journal of Chemistry*, vol. 2013, Article ID 412079, 6 pages, 2013.
- [4] N. Jones, B. Ray, K. T. Ranjit, and A. C. Manna, "Antibacterial activity of ZnO nanoparticle suspensions on a broad spectrum of microorganisms," *FEMS Microbiology Letters*, vol. 279, no. 1, pp. 71–76, 2008.
- [5] S. Arokiyaraj, M. Saravanan, N. K. U. Prakash et al., "Enhanced antibacterial activity of iron oxide magnetic nanoparticles treated with *Argemone mexicana* L. leaf extract: an *in vitro* study," *Materials Research Bulletin*, vol. 48, no. 9, pp. 3323–3327, 2013.
- [6] R. Prucek, J. Tuček, M. Kilianová et al., "The targeted antibacterial and antifungal properties of magnetic nanocomposite of iron oxide and silver nanoparticles," *Biomaterials*, vol. 32, no. 21, pp. 4704–4713, 2011.
- [7] W. Zhang, X. Shi, J. Huang et al., "Bacitracin-conjugated superparamagnetic iron oxide nanoparticles: synthesis, characterization and antibacterial activity," *ChemPhysChem*, vol. 13, no. 14, pp. 3388–3396, 2012.
- [8] E. H. Kim, H. S. Lee, B. K. Kwak, and B.-K. Kim, "Synthesis of ferrofluid with magnetic nanoparticles by sonochemical method for MRI contrast agent," *Journal of Magnetism and Magnetic Materials*, vol. 289, pp. 328–330, 2005.
- [9] T. Hyeon, S. S. L. Su Seong Lee, J. Park, Y. Chung, and H. B. N. Hyon Bin Na, "Synthesis of highly crystalline and monodisperse maghemite nanocrystallites without a size-selection process," *Journal of the American Chemical Society*, vol. 123, no. 51, pp. 12798–12801, 2001.
- [10] F. Fievet, J. P. Lagier, B. Blin, B. Beaudoin, and M. Figlarz, "Homogeneous and heterogeneous nucleations in the polyol process for the preparation of micron and submicron size metal particles," *Solid State Ionics*, vol. 32–33, no. 1, pp. 198–205, 1989.
- [11] H. R. Khan and K. Petrikowski, "Anisotropic structural and magnetic properties of arrays of Fe<sub>26</sub>Ni<sub>74</sub> nanowires electrodeposited in the pores of anodic alumina," *Journal of Magnetism and Magnetic Materials*, vol. 215, pp. 526–528, 2000.
- [12] R. M. Cornell and U. Schertmann, *Iron Oxides in the Laboratory: Preparation and Characterization*, VCH, Weinheim, Germany, 1991.
- [13] D. H. Napper, "Flocculation studies of sterically stabilized dispersions," *Journal of Colloid And Interface Science*, vol. 32, no. 1, pp. 106–114, 1970.
- [14] G. Fritz, V. Schädler, N. Willenbacher, and N. J. Wagner, "Electrosteric stabilization of colloidal dispersions," *Langmuir*, vol. 18, no. 16, pp. 6381–6390, 2002.
- [15] S. Wagner, J. Schnorr, H. Pilgrimm, B. Hamm, and M. Taupitz, "Monomer-coated very small superparamagnetic iron oxide particles as contrast medium for magnetic resonance imaging: preclinical *in vivo* characterization," *Investigative Radiology*, vol. 37, no. 4, pp. 167–177, 2002.
- [16] M. Taupitz, S. Wagner, J. Schnorr et al., "Phase I clinical evaluation of citrate-coated monocrystalline very small superparamagnetic iron oxide particles as a new contrast medium for magnetic resonance imaging," *Investigative Radiology*, vol. 39, no. 7, pp. 394–405, 2004.

- [17] Y. Sahoo, H. Pizem, T. Fried et al., "Alkyl phosphonate/phosphate coating on magnetite nanoparticles: a comparison with fatty acids," *Langmuir*, vol. 17, no. 25, pp. 7907–7911, 2001.
- [18] M. D. Alcalá and C. Real, "Synthesis based on the wet impregnation method and characterization of iron and iron oxide-silica nanocomposites," *Solid State Ionics*, vol. 177, no. 9–10, pp. 955–960, 2006.
- [19] J. Lin, W. Zhou, A. Kumbhar et al., "Gold-coated iron (Fe@Au) nanoparticles: synthesis, characterization, and magnetic field-induced self-assembly," *Journal of Solid State Chemistry*, vol. 159, no. 1, pp. 26–31, 2001.
- [20] L. M. Lacava, Z. G. M. Lacava, M. F. da Silva et al., "Magnetic resonance of a dextran-coated magnetic fluid intravenously administered in mice," *Biophysical Journal*, vol. 80, no. 5, pp. 2483–2486, 2001.
- [21] H. Xu, F. Yan, E. E. Monson, and R. Kopelman, "Room-temperature preparation and characterization of poly(ethylene glycol)-coated silica nanoparticles for biomedical applications," *Journal of Biomedical Materials Research A*, vol. 66, no. 4, pp. 870–879, 2003.
- [22] M. Chastellain, A. Petri, and H. Hofmann, "Particle size investigations of a multistep synthesis of PVA coated superparamagnetic nanoparticles," *Journal of Colloid and Interface Science*, vol. 278, no. 2, pp. 353–360, 2004.
- [23] H.-L. Ma, X.-R. Qi, Y. Maitani, and T. Nagai, "Preparation and characterization of superparamagnetic iron oxide nanoparticles stabilized by alginate," *International Journal of Pharmaceutics*, vol. 333, no. 1–2, pp. 177–186, 2007.
- [24] L. Zhu, J. Ma, N. Jia, Y. Zhao, and H. Shen, "Chitosan-coated magnetic nanoparticles as carriers of 5-Fluorouracil: preparation, characterization and cytotoxicity studies," *Colloids and Surfaces B: Biointerfaces*, vol. 68, no. 1, pp. 1–6, 2009.
- [25] M. Licciardi, C. Scialabba, C. Fiorica et al., "Polymeric nanocarriers for magnetic targeted drug delivery: preparation, characterization, and *in vitro* and *in vivo* evaluation," *Molecular Pharmaceutics*, vol. 10, no. 12, pp. 4397–4407, 2013.
- [26] M. Licciardi, C. Scialabba, G. Cavallaro et al., "Cell uptake enhancement of folate targeted polymer coated magnetic nanoparticles," *Journal of Biomedical Nanotechnology*, vol. 9, no. 6, pp. 949–964, 2013.
- [27] Y. Park, R. D. Whitaker, R. J. Nap et al., "Stability of superparamagnetic iron oxide nanoparticles at different pH values: experimental and theoretical analysis," *Langmuir*, vol. 28, no. 15, pp. 6246–6255, 2012.
- [28] C. Hoskins, A. Cuschieri, and L. Wang, "The cytotoxicity of polycationic iron oxide nanoparticles: common endpoint assays and alternative approaches for improved understanding of cellular response mechanism," *Journal of Nanobiotechnology*, vol. 10, p. 15, 2012.
- [29] S. B. Zotchev, "Polyne macrolide antibiotics and their applications in human therapy," *Current Medicinal Chemistry*, vol. 10, no. 3, pp. 211–223, 2003.
- [30] J. M. T. Hamilton Miller, "Chemistry and biology of the polyene macrolide antibiotics," *Bacteriological Reviews*, vol. 37, no. 2, pp. 166–196, 1973.
- [31] M. S. Usman, M. E. El Zowalaty, and K. Shameli, "Synthesis, characterization, and antimicrobial properties of copper nanoparticles," *International Journal of Nanomedicine*, vol. 8, pp. 4467–4479, 2013.
- [32] J. M. Andrews, "BSAC standardized disc susceptibility testing method," *Journal of Antimicrobial Chemotherapy*, vol. 48, supplement 1, pp. 43–57, 2001.
- [33] M. S. Al-Qubaisi, A. Rasedee, M. H. Flaifel et al., "Cytotoxicity of NiZn ferrite nanoparticles on cancer cells of epithelial origin," *International Journal of Nanomedicine*, vol. 8, pp. 2497–2508, 2013.
- [34] A. Zhu, L. Yuan, and T. Liao, "Suspension of  $\text{Fe}_3\text{O}_4$  nanoparticles stabilized by chitosan and o-carboxymethylchitosan," *International Journal of Pharmaceutics*, vol. 350, no. 1–2, pp. 361–368, 2008.
- [35] R. H. Marchessault, F. Ravenelle, and X. X. Zhu, *Polysaccharides for Drug Delivery and Pharmaceutical Applications*, vol. 934, An American Chemical Society, 2006.
- [36] J. Lodhia, G. Mandarano, N. J. Ferris, P. Eu, and S. F. Cowell, "Development and use of iron oxide nanoparticles—part 1: synthesis of iron oxide nanoparticles for MRI," *Biomedical Imaging and Intervention Journal*, vol. 6, no. 2, pp. 1–11, 2010.
- [37] M. Yamaura, R. L. Camilo, L. C. Sampaio, M. A. Macêdo, M. Nakamura, and H. E. Toma, "Preparation and characterization of (3-aminopropyl)triethoxysilane-coated magnetite nanoparticles," *Journal of Magnetism and Magnetic Materials*, vol. 279, no. 2–3, pp. 210–217, 2004.
- [38] K. J. Sreeram, M. Nidhin, R. Indumathy, and B. U. Nair, "Synthesis of iron oxide nanoparticles of narrow size distribution on polysaccharide templates," *Bulletin of Materials Science*, vol. 31, no. 1, pp. 93–96, 2008.
- [39] S. Yu and C. M. Chow, "Carboxyl group ( $-\text{CO}_2\text{H}$ ) functionalized ferrimagnetic iron oxide nanoparticles for potential bio-applications," *Journal of Materials Chemistry*, vol. 14, no. 18, pp. 2781–2786, 2004.
- [40] L. Dong, L. Yan, W.-G. Hou, and S.-J. Liu, "Synthesis and release behavior of composites of camptothecin and layered double hydroxide," *Journal of Solid State Chemistry*, vol. 183, no. 8, pp. 1811–1816, 2010.
- [41] Y.-S. Ho and A. E. Ofomaja, "Pseudo-second-order model for lead ion sorption from aqueous solutions onto palm kernel fiber," *Journal of Hazardous Materials*, vol. 129, no. 1–3, pp. 137–142, 2006.
- [42] T. Higuchi, "Mechanism of sustained action medication. Theoretical analysis of rate of release of solid drugs dispersed in solid matrices," *Journal of Pharmaceutical Sciences*, vol. 52, no. 12, pp. 1145–1149, 1963.
- [43] A. W. Hixson and J. H. Crowell, "Dependence of reaction velocity upon surface and agitation," *Industrial & Engineering Chemistry*, vol. 23, no. 8, pp. 923–931, 1931.
- [44] R. W. Korsmeyer, R. Gurny, and E. Doelker, "Mechanisms of solute release from porous hydrophilic polymers," *International Journal of Pharmaceutics*, vol. 15, no. 1, pp. 25–35, 1983.